Localized and mobile electrons in metal - molten-salt solutions

1996 J. Phys.: Condens. Matter 8 9309

(http://iopscience.iop.org/0953-8984/8/47/021)

J. Phys.: Condens. Matter **8** (1996) 9309–9314. Printed in the UK

Localized and mobile electrons in metal–molten-salt solutions

D Nattland, B von Blanckenhagen, R Juchem, E Schellkes and W Freyland

Institute of Physical Chemistry and Electrochemistry, University of Karlsruhe, D-76128 Karlsruhe, Germany

Received 15 July 1993

Abstract. At elevated temperatures (about 10^3 K) liquid alkali metal–alkali halide solutions transform continuously from the nonmetallic to the metallic state (NM–M transition) as a function of the metal mole fraction x_M. In this study we present results of new experiments on spectroscopic ellipsometry and on absorption spectroscopy across the transition regime. The data indicate that on both sides of the NM–M transition localized and mobile electronic states may coexist

1. Introduction

Alkali metal–alkali halide fluids exhibit a drastic change in homogeneous phase with varying metal concentration from an ionic conducting liquid salt to an electronic conducting liquid metal [1]. In the concentration regime up to $x_M \leqslant 0.05$, when these systems show clearly nonmetallic behaviour, the electronic properties are characterized by strongly localized monomer and dimer species (e.g. F centres and bipolarons) and by weakly bound mobile electrons. The former show distinct optical absorption bands similar to those in the solid state. The latter exhibit a broad structureless absorption feature, whose energy dependence can be described consistently within the Drude model for free electrons. The input parameters μ_e (electronic mobility) and n_e (density of the Drude-type electrons) are in agreement with independent experiments [2, 3].

For the understanding of the nonmetal–metal (NM–M) transition it is essential to know how this interplay between localized states and mobile states develops with the metal concentration and how the electronic mobility increases across the NM–M transition: on the nonmetallic side μ_e is of the order of 0.1 $cm^2\ V^{-1}\ s^{-1}$ in these systems; a typical metallic transport mechanism requires roughly 10 $cm^2\ V^{-1}\ s^{-1}$. These open questions may be elucidated by optical spectroscopic methods. In this study we present results on K–KCl ($0.03 \leqslant x_K \leqslant 0.7$) obtained by spectroscopic ellipsometry and on Cs–CsI ($0 \leqslant x_{Cs} \leqslant 0.25$ obtained by absorption spectroscopy.

2. Experimental procedure

In both experiments emphasis was given to the precise *in situ* variation of the metal mole fraction under high-temperature conditions at 800 °C. This was studied by the combination of the optical cells with electrochemical cells which work according to the following reversible

0953-8984/96/479309+06$19.50

EMF cell [4]:

$Ca–Sn(l)|CaF_2(s)|MCaF_3(s)–M(v)$ (M: K, Cs) (s, l, v: solid, liquid, vapour).

If a cathodic potential is applied to the right-hand side of the electrochemical cell may now fit, M^+ is reduced to M in solid $MCaF_3$ and in the equilibrium vapour phase. The alkali metal vapour equilibrates with the liquid alkali halide to achieve a uniform chemical potential measured by the EMF. Integration of the current passing through the cell gives the number density of excess metal in the liquid salt which connects the spectroscopic characteristics to the thermodynamic properties. At high potassium compositions ($0.46 \leqslant x_K \leqslant 0.70$) a different approach was used: a steel bellow, sealed with a tantalum foil and filled with potassium, was vacuum-tight connected to the optical part. By squeezing the bellow a steel needle moved against the Ta membrane and opened a path for the potassium vapour to the optical compartment of the cell.

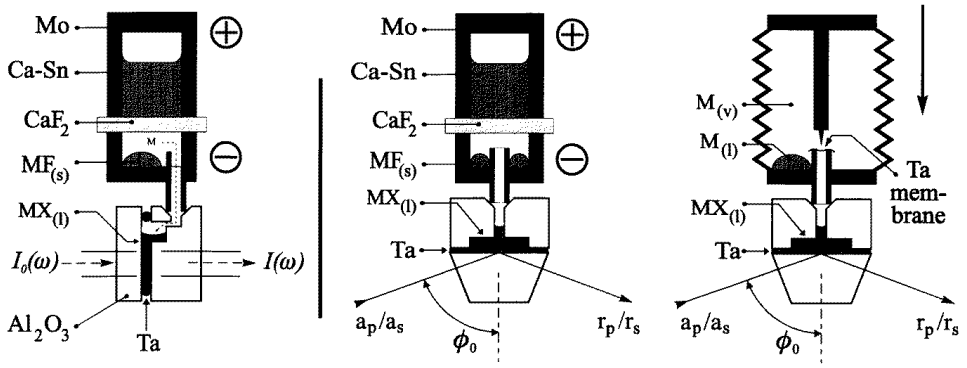

Figure 1. A schematic representation of the optical cells. Left: the electrochemical cell consisting of the Ca–Sn reference electrode, CaF_2 solid-state electrolyte, working electrode and absorption cell consisting of two sapphire plates sealed with Ta wires. At the given polarity the MF (or $MCaF_3$) in the working electrode is reduced. Middle: the electrochemical cell and ellipsometric cell consisting of a sapphire plate and a sapphire prism as the window. Also shown are the angle of incidence ϕ_0, and the incoming a_p, a_s and reflected r_p, r_s amplitudes of the parallel and normal components of the electric field vector. Ellipsometry measures the ratio and phase-shift of r_p and r_s yielding the complex dielectric function $\epsilon = \epsilon_1 - i\epsilon_2$. Right: the bellow–needle cell for high metal concentrations.

The high-temperature optical cells had to be made of sapphire for corrosion reasons. Details of the cells and of the spectrometer set-up have been described elsewhere [2, 5]. They are schematically represented in figure 1. The usage of sapphire in an ellipsometric experiment is crucial due to its birefringent properties. For this the ellipsometric phase-shift parameter Δ had to be calibrated carefully at the sapphire–molten-salt interface at constant temperature. Subsequent metal doping—either performed electrochemically or by the bellow–needle method—was measured with reference to this calibration [5]. This procedure requires long-term temperature stability of 10^{-2} K over several days, which is very difficult to achieve. Thus we estimate the absolute error of the real and imaginary parts of the dielectric function, ϵ_1 and ϵ_2, to be approximately 30% to 50%.

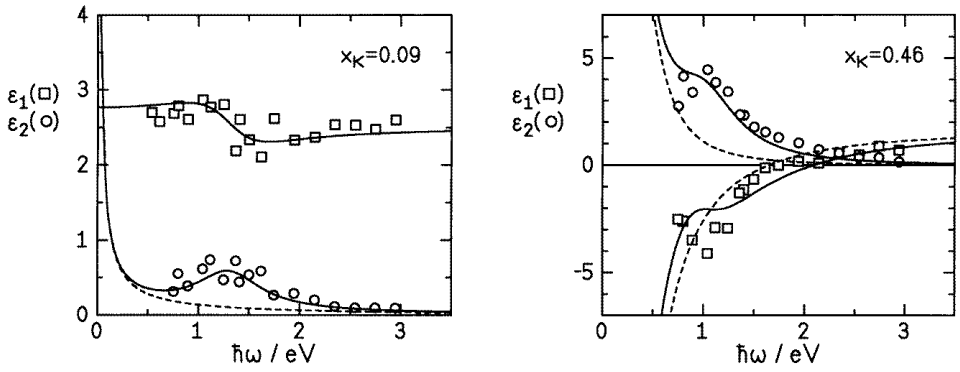

Figure 2. Typical ellipsometric spectra of K–KCl. Solid lines: Drude–Lorentz model; dashed lines: Drude contribution solely. For further details see the text.

3. Results and discussion

Typical ellipsometric spectra of ϵ_1 and ϵ_2 are presented in figure 2 for two compositions.

At $x_K = 0.09$, ϵ_2 clearly shows outside the experimental uncertainties a broad absorption band with a maximum between 1 eV and 1.5 eV and an estimated half-width of 0.5 eV to 1 eV. This is also reflected in the dispersion behaviour of ϵ_1. The solid lines correspond to a calculation of the spectra assuming a Drude-type contribution and a single Lorentzian oscillator. The dashed lines show the underlying Drude electron part separately, which was fixed by the measured DC conductivity (σ_0) [6]. The number densities of both Drude (n_D) and Lorentz (n_L) contributions were adjusted by the given mole fraction assuming an oscillator strength of one for the latter. Calculations were made on the one hand for strongly localized monomer states (e.g. F centres) and on the other hand for dimer states like bipolarons to take into account the strong tendency of the system to form diamagnetic species [7]. In both cases the agreement is reasonable. This, of course, affects the calculated electronic mobility ($\mu_e = \sigma_0 e^{-1} n_D^{-1}$), which can be determined from this analysis with an accuracy of a factor of two.

At $x_K = 0.46$ the shape of the spectra have changed substantially. The real part ϵ_1 is negative below 2 eV due to the higher electronic conductivity and the higher concentration of nearly free electrons. Again, the Drude contribution is given as a dashed line. It can be clearly seen that this contribution is not sufficient for the interpretation of the spectra. ϵ_2 shows a broad absorption band centred at around 1 eV. This is remarkable since at this composition the system is in its metallic state [1]. A Drude–Lorentz model is given by the solid lines in the right-hand panel of figure 2. The nature of the states leading to the absorption pattern besides the free-electron part is not clear yet. Neutron diffraction studies show that ionic charge ordering as a fingerprint for molten alkali halides is still present in this concentration regime [8]. So, it might be that deep trap states comparable to the F centres or bipolarons in the nonmetallic regime persist on the metallic side of the NM–M transition. This reminds one of the situation discussed for optical excitations in metallic Si:P [9].

Ellipsometric spectra are valuable for direct comparison with recent *ab initio* molecular dynamics calculations on M–MX solutions [10]. At first glance, the agreement of our spectra with the calculated ones for $x \leqslant 0.2$ is satisfactory at energies above 1.2 eV, whereas at

lower energies the QMD spectra clearly deviate to higher values of ϵ_2. From this one would expect that according to the QMD calculations the NM–M transition occurs at metal concentrations lower than the experimental one. A more detailed comparison will be given in the near future.

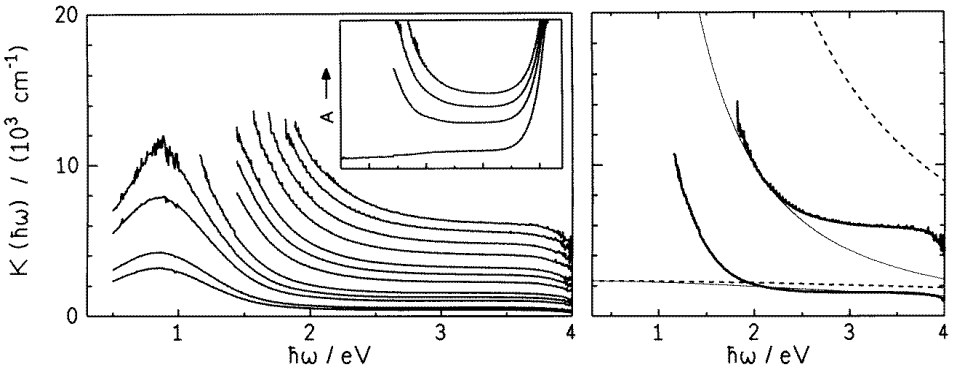

Figure 3. Left-hand panel: absorption spectra of Cs–CsI at the following concentrations, x_{Cs}: 0.010, 0.012, 0.023, 0.027, 0.039, 0.065, 0.082, 0.098, 0.133, 0.168, 0.209, 0.250. Inset: original data for pure CsI and $x_{Cs} = 0.065$, 0.115, 0.168. Right-hand panel: $x_{Cs} = 0.039$ and 0.229. Included are calculations of the Drude contribution; for further details see the text.

In the left-hand panel of figure 3 new absorption spectra for Cs–CsI are presented. They cover the concentration range $0.01 \leqslant x_{Cs} \leqslant 0.25$ and were recorded in a single experimental run. In the inset of this figure the spectrum of the pure salt and the spectra of three metal–salt mixtures at three different compositions are shown as raw data. The strong absorption of the fundamental edge is clearly seen around 4 eV. Subtraction of the salt spectrum from those with metal doping eliminates all parasitic effects of the experimental set-up, thus leading to the high-quality spectra of figure 3. These show a broad absorption band centred at 0.844 eV (half-width 0.91 eV; for details of the measurements and the data evaluation see reference [2]) which is attributed to the first electronic excitation of the strongly localized F centres or bipolarons. At compositions above $x_{Cs} = 0.024$ this band exceeds the absorbance range accessible in our experimental set-up. Besides this dominant absorption, a structureless background contribution with only weak energy dependence is clearly visible. This contribution was found to be consistent with the Drude formalism in K–KCl, Na–NaBr and Na–NaI in the concentration range up to $x_M \approx 0.05$. The corresponding electronic mobility is of the order of 0.1 $cm^2\ V^{-1}\ s^{-1}$ and the measured DC conductivity is reproduced within the experimental error [2].

Towards higher concentrations, i.e. across the NM–M transition, the situation gets more complicated. This is demonstrated in the right-hand panel of figure 3: it shows two spectral sections for $x_{Cs} = 0.039$ and for $x_{Cs} = 0.229$. Both spectra have been adapted to the Drude formalism with fixed conductivities of 6.2 $\Omega^{-1}\ cm^{-1}$ and 207 $\Omega^{-1}\ cm^{-1}$, respectively [11]. The only parameter for adjustment is the number density of Drude electrons n_D. At low metal concentration n_D is not very sensitive to the shape of the spectra. The dashed line shows the shape of the calculated Drude absorption if all excess electrons were to participate in this transport process ($n_D = 0.267 \times 10^{21}\ cm^{-3}$). The thin solid line—fit results for $n_D = 0.15 \times 10^{21}\ cm^{-3}$—is in good agreement with the spectrum at energies above 2.0 eV. The situation completely changes at higher concentration. Again, for reference the dashed line shows the spectral characteristics considering all excess electrons as free

electrons (here: $n_D = 1.55 \times 10^{21}$ cm^{-3}). This clearly overestimates the absorptivity of that particular Cs–CsI sample in the energy range considered. On the other hand a number density of $n_D = 0.79 \times 10^{21}$ cm^{-3} is consistent with the spectrum but, surprisingly, now the Drude *ansatz* does not describe the plateau-like part. It approaches the low-energy part *below* 2.2 eV. The additional absorption above this value might be due to excitations from trap states into the conduction band. A similar observation was made for Na–NaI [2].

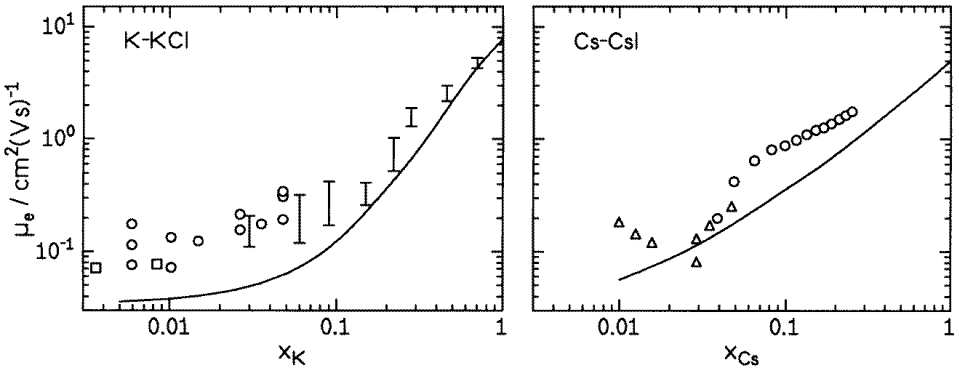

Figure 4. Electronic mobility as obtained by different experimental methods. For further details see the text.

We are aware that our simple two-component model with localized and free-electron states cannot cover the drastic change of the electronic properties in going from a nonmetal to a metal. Nevertheless, it may help to estimate the maximum number density of electrons participating in the conduction process. This in turn allows one to calculate the electronic mobility and its evolution with composition. This has been done for the ellipsometric spectra of K–KCl and for the absorption spectra of Cs–CsI as shown in figure 4. The solid lines in the left-hand and right-hand panels of figure 4 demonstrate the trivial case, assuming all excess electrons being present as conduction electrons, yielding μ_e directly from measured σ-data [6, 11]. For a given composition this fixes the lower limit of the electronic mobility. In the M–MX systems the DC conductivity typically ranges from $10^0\ \Omega^{-1}$ cm^{-1} in the pure salts to $10^4\ \Omega^{-1}$ cm^{-1} in pure metals. The typical value for the NM–M transition regime of $10^2\ \Omega^{-1}$ cm^{-1} is reached at around $x_M \approx 0.2$.

The squares in the left-hand part of figure 4 correspond to the only direct measurement of the electronic mobility obtained from polarization experiments [3]. Circles give results of fits to absorption spectra of K–KCl [2, 12] which show a slight increase of μ_e by a factor of two up to $x_K \approx 0.05$. The bars represent mobilities extracted from the Drude–Lorentz fits to the ellipsometric spectra as mentioned above. μ_e increases in the concentration range up to $x_K = 0.15$ by roughly a factor of two reaching a value of 0.3 to 0.4 cm^2 V^{-1} s^{-1}. Above this concentration a steeper increase leads to $\mu_e = 1$ cm^2 V^{-1} s^{-1} at around $x_K = 0.2$. Together with the DC conductivity of 100 Ω^{-1} cm^{-1} this is consistent with electronic transport in extended states, i.e. the system is now metallic [13].

In the right-hand panel of figure 4 a similar data evaluation is shown for the absorption spectrum of Cs–CsI for two different series of spectra. Unfortunately, there are no direct measurements of the mobility available. The initial decrease of the data marked with triangles is an artefact and gives a first hint that it is not only Drude electrons that contribute to the absorption at high energies. The mobilities at higher concentrations have been

obtained from estimates of the maximum numbers of Drude electrons as has been stated in the discussion of figure 3. μ_e increases to a value of 1 $cm^2\ V^{-1}\ s^{-1}$ in a concentration range up to $x_{Cs} = 0.1$. Above this concentration the electronic mobility seems to approach smoothly the value of pure liquid caesium for these conditions. Finally the mobility in both cases is found to be higher than in the trivial case. This again indicates that a considerable number of excess electrons do not participate in the conduction process and are possibly localized in trapped states even in the metallic regime. In conclusion, the interpretation of the spectroscopic results of different alkali metal–alkali halide melts within a simple two-component model leads to a consistent description of the electronic mobility behaviour across the NM–M transition.

References

[1] Freyland W 1994 *Z. Phys. Chem.* **184** 139; 1995 *Metal–Insulator Transition Revisited* ed P P Edwards and C N R Rao (London: Taylor and Francis) p 167

[2] Nattland D, Rauch T and Freyland W 1993 *J. Chem. Phys.* **98** 4429
von Blanckenhagen B, Nattland D and Freyland W 1994 *J. Phys.: Condens. Matter* **6** L179

[3] Haarberg G M and Egan J J 1996 *Proc. 189th Mtg of the Electrochemical Society (10th Int. Symp. on Molten Salts); J. Electrochem. Soc.*

[4] Bernard J, Blessing J, Schummer J and Freyland W 1993 *Ber. Bunsenges. Phys. Chem.* **97** 177

[5] Juchem R 1995 *PhD Thesis* University of Karlsruhe
Schellkes E 1994 *Diploma Thesis* University of Karlsruhe

[6] Bronstein H R and Bredig M A 1958 *J. Am. Chem. Soc.* **80** 2077
Nattland D, Heyer H and Freyland W 1986 *Z. Phys. Chem.* **149** 1

[7] Schindelbeck T and Freyland W 1996 *J. Chem. Phys.* **105** 4448

[8] Jal J F, Mathieu C, Chieux P and Dupuy J 1990 *Phil. Mag.* B **62** 351
Hily L, Dupuy J, Jal J F and Chieux P 1994 *Rev. Int. Hautes Temp. Réfract., Fr.* **29** 1

[9] Gaymann A, Geserich H P and von Löhneysen H 1993 *Phys. Rev. Lett.* **71** 3681
Holcomb D F 1995 *Metal–Insulator Transition Revisited* ed P P Edwards and C N R Rao (London: Taylor and Francis) p 65

[10] Silvestrelli P L, Alavi A, Parrinello M and Frenkel D 1996 *Phys. Rev.* B **53** 12 750

[11] Sotier S and Jäger W 1988 *Z. Phys. Chem.* **156** 203

[12] Nattland D 1996 *Habilitation* University of Karlsruhe

[13] Mott N F and Davis E A 1977 *Electronic Processes in Non-Crystalline Materials* (Oxford: Clarendon)